Tests of a compact static Fourier-transform imaging spectropolarimeter

Jie Li,* Bo Gao, Chun Qi, Jingping Zhu, and Xun Hou

School of Electronics & Information Engineering, Xi'an Jiaotong University, Xi'an 710049, China simonli139@gmail.com

Abstract: A compact Fourier-transform imaging spectropolarimeter covering a 450-1000 nm spectral range is presented. The sensor, which is based on two birefringent retarders and a Wollaston interferometer, offers significant advantages over previous implementations. Specifically, with no internal moving parts, electrically controllable or micro polarization components, the full wavelength-dependent state of polarization, spectral and spatial information of a scene can be acquired simultaneously. Outdoor measurements of several cars and plants demonstrate the sensor's potential for color measurement, target identification, and agriculture monitoring applications.

©2014 Optical Society of America

OCIS codes: (110.4234) Multispectral and hyperspectral imaging; (120.6200) Spectrometers and spectroscopic instrumentation; (120.5410) Polarimetry.

References and links

- W. Groner, J. W. Winkelman, A. G. Harris, C. Ince, G. J. Bouma, K. Messmer, and R. G. Nadeau, "Orthogonal polarization spectral imaging: A new method for study of the microcirculation," Nat. Med. 5(10), 1209-1212
- N. J. Pust and J. A. Shaw, "Wavelength dependence of the degree of polarization in cloud-free skies: simulations of real environments," Opt. Express 20(14), 15559-15568 (2012).
- T. G. Moran and J. M. Davila, "Three-dimensional polarimetric imaging of coronal mass ejections," Science 305(5680), 66-70 (2004).
- J. S. Tyo, D. L. Goldstein, D. B. Chenault, and J. A. Shaw, "Review of passive imaging polarimetry for remote sensing applications," Appl. Opt. 45(22), 5453-5469 (2006).
- X. Meng, J. Li, T. Xu, D. Liu, and R. Zhu, "High throughput full Stokes Fourier transform imaging
- spectropolarimetry," Opt. Express **21**(26), 32071–32085 (2013).

 T. Mu, C. Zhang, C. Jia, and W. Ren, "Static hyperspectral imaging polarimeter for full linear Stokes parameters," Opt. Express 20(16), 18194-18201 (2012).
- M. H. Smith, J. B. Woodruff, and J. D. Howe, "Beam wander considerations in imaging polarimetry," Proc. SPIE 3754, 50-54 (1999).
- A. Bénière, M. Alouini, F. Goudail, and D. Dolfi, "Design and experimental validation of a snapshot polarization contrast imager," Appl. Opt. 48(30), 5764-5773 (2009).
- M. W. Kudenov, M. E. L. Jungwirth, E. L. Dereniak, and G. R. Gerhart, "White light Sagnac interferometer for snapshot linear polarimetric imaging," Opt. Express 17(25), 22520-22534 (2009).
- 10. K. Oka and T. Kato, "Spectroscopic polarimetry with a channeled spectrum," Opt. Lett. 24(21), 1475-1477
- 11. D. Sabatke, A. Locke, E. L. Dereniak, M. Descour, J. Garcia, T. Hamilton, and R. W. McMillan, "Snapshot imaging spectropolarimeter," Opt. Eng. 41(5), 1048-1054 (2002).
- 12. S. H. Jones, F. J. Iannarilli, and P. L. Kebabian, "Realization of quantitative-grade fieldable snapshot imaging spectropolarimeter," Opt. Express 12(26), 6559-6573 (2004).
- 13. K. Oka and T. Kaneko, "Compact complete imaging polarimeter using birefringent wedge prisms," Opt. Express 11(13), 1510-1519 (2003).
- 14. M. W. Kudenov, N. A. Hagen, E. L. Dereniak, and G. R. Gerhart, "Fourier transform channeled spectropolarimetry in the MWIR," Opt. Express 15(20), 12792-12805 (2007).
- 15. J. Craven-Jones, M. W. Kudenov, M. G. Stapelbroek, and E. L. Dereniak, "Infrared hyperspectral imaging polarimeter using birefringent prisms," Appl. Opt. 50(8), 1170–1185 (2011).
- J. Li, J. Zhu, and H. Wu, "Compact static Fourier transform imaging spectropolarimeter based on channeled polarimetry," Opt. Lett. **35**(22), 3784–3786 (2010).

1. Introduction

An imaging spectropolarimeter (ISP, also called a hyperspectral imaging polarimeter) is a combination of an imaging device (a digital camera), a spectrometer and a polarimeter. The obtained data set contains four independent "datacubes". Each one is a 3D matrix formed by a 2D spatial image combined with a third dimension that is one of the wavelength dependent Stokes parameter $S_i(\sigma)$ (i is the set of integers from 0 to 3) of each pixel of the image, respectively. The wavelength dependent Stokes parameters are defined by

$$\mathbf{S}_{i}(\sigma) = \begin{bmatrix} S_{0}(\sigma) \\ S_{1}(\sigma) \\ S_{2}(\sigma) \\ S_{3}(\sigma) \end{bmatrix} = \begin{bmatrix} I_{0}(\sigma) + I_{90}(\sigma) \\ I_{0}(\sigma) - I_{90}(\sigma) \\ I_{445}(\sigma) - I_{-45}(\sigma) \\ I_{R}(\sigma) - I_{L}(\sigma) \end{bmatrix}, \tag{1}$$

where the σ is wave number. S_0 is the total intensity of the light, while S_1 denotes the part of 0° linear polarized light over 90°, S_2 for + 45° over -45°, and S_3 for right circular over left circular. These four parameters can describe the complete polarization state of light at a given spectral band.

ISP device has rapidly developed in recent years, and become a well recognized technique in many fields, including biomedical diagnosis [1], environment monitoring [2], space exploration [3], remote sensing [4], and other scientific areas, as a powerful tool for object detection and identification with preferable accuracy.

However, in conventional imaging spectropolarimeters, polarization analyzing optics such as, rotating polarization elements, electrically controllable components, and microretarder or micropolarizer arrays are typically used together with an imaging spectrometer. Both of the polarization analyzing optics and imaging spectrometer must be scanned in the measurements. These apparatuses generally suffer from vibration, electrical noise, heat generation, and alignment difficulty. Consequently, considerable care is required for stable operation. Additionally, the incorporation of mechanical components typically increases the complexity and decreases the reliability of the measurement system.

Recently, several improving aperture/amplitude division methods were proposed to modulate the Stokes parameters into the imaging spectrometer by using relatively simple polarized arrays and lens arrays [5, 6]. However, differences in distortion, focal length, and transmission coefficient of the optics necessitate sophisticated image registration algorithms [7–9]. Besides, since the imaging area of the sensor is divided into several sub-areas, the obtained spatial resolution is severely reduced.

The channeled polarimetric technique [10] is an attractive approach for polarimetry. Based on this concept, a variety of different types of polarimeters have been developed for capturing polarization states of light [11–15]. K. Oka et al. developed an imaging polarimeter constructed by several birefringent wedge prisms employing monochromatic illumination [13]. Kudenov et al. provided a non-imaging spectropolarimeter in the middle wave infrared (MWIR) [14]. Very recently, Jones proposed an infrared hyperspectral imaging polarimeter (IHIP) based on a birefringent wedge moving interferometer [15]. The main drawback is its internal mechanical moving parts and poor temporal registration for rapidly changing scenesespecially for remote sensing applications on moving platforms.

In this paper, we report a compact static Fourier-transform imaging spectropolarimeter (FTISP) combined channeled polarimetry with a Wollaston prism interferometer. Without any internal moving parts, electrically controllable or micro-components, the entire wavelength-dependent state of polarization (SOP), spectral and spatial information of a scene can be acquired simultaneously [16]. The presented system is kept simple, compact and rugged with its optical performances and applicability proved to be powerful and practical for laboratory and field applications.

2. Theories

2.1 Instrument setup

The schematic setup of the FTISP system is illustrated in Fig. 1. It comprises a fore-optics, two birefringent crystal retarders, R_1 and R_2 with thicknesses d_1 and d_2 , respectively, a polarizer P, a Wollaston prism WP, an analyzer A, a reimaging lenses L and a digital CCD camera. The fast axes of R_1 and R_2 are oriented at 45° and 0°, respectively, relative to the x-axis, and the transmission axis of P is aligned with the fast axis of R_1 .

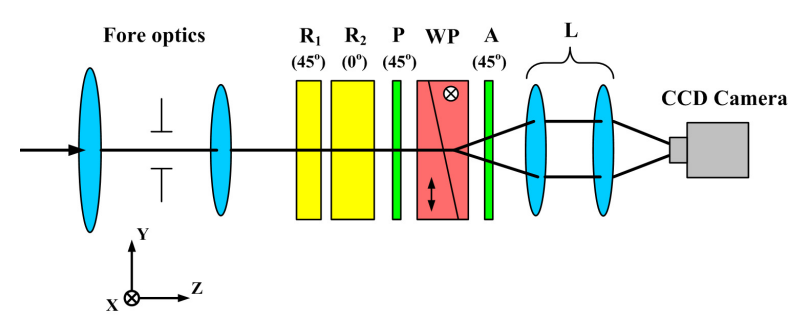


Fig. 1. Schematic setup of the FTISP system.

Light from a scene is collected and collimated by fore-optics, and then passes through R_1 , R_2 and P. Light emerging from P becomes linearly polarized at 45° to the optic axes of WP. WP splits the incoming light into two equal amplitude, orthogonally polarized components with a small divergent angle. After passing through A, the two component rays are resolved into linearly polarized light in the same orientation and recombined onto the camera by L. The camera then records interferogram patterns along one dimension (rows) and spatial imaging (1D) of the scene along the other dimension (columns) within a single snapshot. This mode of data acquisition is the so-called "push-broom" mode, in which 2D spatial imaging is derived by scanning the sensor across a scene.

2.2 Operation principle

The obtained interferogram of the FTISP can be calculated by using the Mueller matrix theory [10, 14]. We assume that the light from the object has a broadband spectrum, and gradually changes with wave number σ from σ_1 to σ_2 . So the interferogram I(z) can be described as [16]:

$$I(z) = \int_{\sigma_i}^{\sigma_i} I(z, \sigma) d\sigma = \int_{\sigma_i}^{\sigma_i} \mathbf{M}_s \mathbf{S}_i(\sigma) d\sigma,$$
 (2)

where z denotes the path difference introduced by the interferometer. \mathbf{M}_s characterizes the collective polarimetric response of the sensor's polarization elements, and can be given by:

$$\mathbf{M}_{s} = \mathbf{M}_{A} \mathbf{M}_{W} \mathbf{M}_{P} \mathbf{M}_{R_{A}} \mathbf{M}_{R_{A}}, \tag{3}$$

where \mathbf{M}_A , \mathbf{M}_W , \mathbf{M}_P , \mathbf{M}_{R_2} and \mathbf{M}_{R_1} are the Mueller matrices of the analyzer, the Wollaston prism, the polarizer, the retarders R_2 and R_1 , respectively. Thus, the obtained interferogram, which is the first row of the Stokes vector of the transmitted light impinging upon the camera, is given by:

$$I(z) = \int_{\sigma_{2}}^{\sigma_{1}} \frac{1 + \cos(\phi_{z}(\sigma))}{4} \begin{cases} S_{0}(\sigma) + \frac{1}{2} S_{2}(\sigma) [\exp(i\phi_{2}(\sigma)) + \exp(-i\phi_{2}(\sigma))] \\ + \frac{1}{4} [S_{13}(\sigma) \exp(i(\phi_{1}(\sigma) - \phi_{2}(\sigma))) \\ + S_{13}^{*}(\sigma) \exp(-i(\phi_{1}(\sigma) - \phi_{2}(\sigma)))] \\ - \frac{1}{4} [S_{13}(\sigma) \exp(i(\phi_{1}(\sigma) + \phi_{2}(\sigma))) \\ + S_{13}^{*}(\sigma) \exp(-i(\phi_{1}(\sigma) + \phi_{2}(\sigma)))] \end{cases}$$

with the phase terms

$$\phi_z(\sigma) = 2\pi\Delta z\sigma,\tag{5}$$

$$\phi_1(\sigma) = 2\pi B(\sigma) d_1 \sigma, \tag{6}$$

$$\phi_2(\sigma) = 2\pi B(\sigma) d_2 \sigma. \tag{7}$$

Where $S_{13}(\sigma) = S_1(\sigma) + iS_3(\sigma)$, and the superscript * denotes the complex conjugate. Δz is the optical path difference (OPD) from the Wollaston prism, while $B(\sigma)$ are the birefringence of the birefringent crystal. From Eq. (4), we can see that different phase factors are modulated onto the Stokes parameters of incident light. Performing the integration over σ , Eq. (4) can be rewritten as:

$$I(z) = \frac{1}{4}C_{0}(z) + \frac{1}{8}C_{2}(z - L_{2}) + \frac{1}{8}C_{2}^{*}(-z - L_{2})$$

$$+ \frac{1}{16}C_{1}(z - (L_{1} - L_{2})) + \frac{1}{16}C_{1}^{*}(-z - (L_{1} - L_{2})).$$

$$- \frac{1}{16}C_{3}(z - (L_{1} + L_{2})) - \frac{1}{16}C_{3}^{*}(-z - (L_{1} + L_{2}))$$
(8)

Here L_1 and L_2 denote the OPD introduced by R_1 and R_2 . It can be shown that the interferogram I(z) is separated into seven channels, centered at z=0, $\pm(L_1-L_2)$, $\pm L_2$, and $\pm(L_1+L_2)$.

By filtering the desired channels and performing the inverse Fourier transform, the incident spectrally-dependent Stokes parameters can be demodulated as:

$$\mathfrak{F}^{-1}(C_0) = \frac{1}{4} S_0(\sigma), \tag{9}$$

$$\mathfrak{F}^{-1}(C_1) = \frac{1}{16} (S_1(\sigma) - jS_3(\sigma)) \exp(j(\phi_2(\sigma) - \phi_1(\sigma))), \tag{10}$$

$$\mathfrak{F}^{-1}(C_2) = \frac{1}{8} S_2(\sigma) \exp(j\phi_2(\sigma)). \tag{11}$$

3. Test experiments

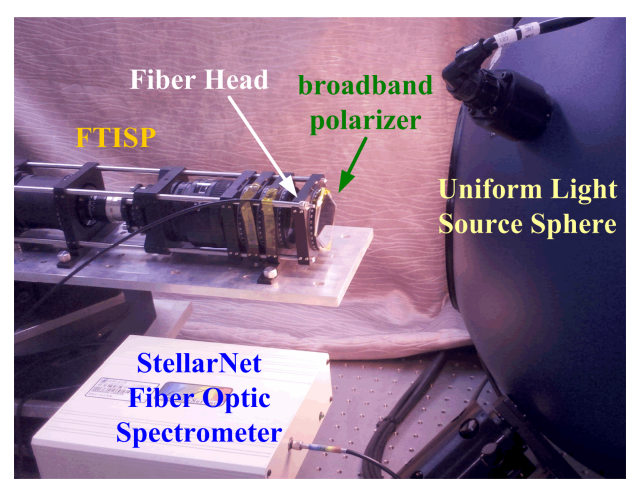
The prototype of the FTISP is shown in Fig. 2. The working spectral range of the system is from 450 nm to 1000 nm. The retarders and Wollaston prism are made of calcite. The thicknesses of R_1 and R_2 are 380 μm and 760 μm with a 1 mm cemented quartz substrate to strengthen the retarders, respectively. The Wollaston prism is 20 mm \times 20 mm \times 5 mm with an internal wedge angle of 5 degrees. A monochromatic 1024 \times 1024 CCD camera with a pixel spacing of 12 μm (DALSA Pantera 1M60) is used to take the interferograms and images of the targets.



Fig. 2. Photograph of the FTISP mounted on a tripod.

3.1 Laboratory tests

To verify the FTISP system's spectropolarimetric capability, the experimental setup shown in Fig. 3 was implemented. A uniform light source integrating sphere (Labsphere) and an ultra broadband wire grid polarizer (Edmund optics) were used to generate the polychromatic light being measured.



 $Fig.\ 3.\ Experiment\ setup\ for\ laboratory\ testing\ of\ the\ FTISP.$

Recovered spectrum from the FTISP system was compared to spectrum acquired using a StellarNet fiber optic spectrometer with a spectral resolution of approximately 5 nm. It should

be indicated that the total intensity $S_0(\sigma)$ is the so called spectrum. This comparison is depicted in Fig. 4(a), while the demodulated wavelength dependent SOP $S_1 \sim S_3$ from the FTISP were compared to the theoretical values of the polarizer shown in Fig. 4(b).

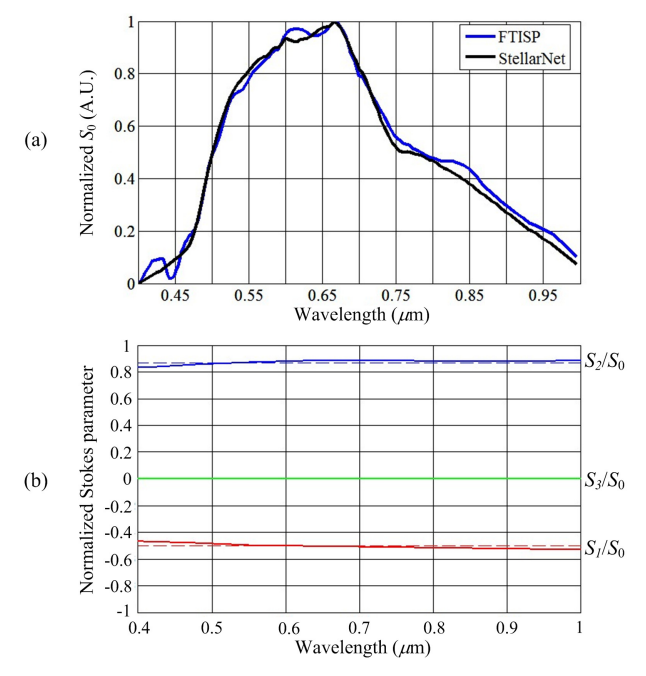


Fig. 4. (a) Spectrum from the FTISP system (blue line) and StellarNet spectrometer (black line). (b) Normalized Stokes parameters. Solid and dashed curves show the experimental and theoretical values, respectively.

In Fig. 4(a), the spectra acquired by the two instruments were normalized in intensity for qualitative comparison. The spectral profiles of the light source demonstrate good agreement. Note that the spectrum from the FTISP system was obtained when the polarizer sample was removed. In Fig. 4(b), compared with the theoretical values, the experimental results of Stokes parameters were shown to yield accuracy better than 3% over most of the 450-1000 nm band. The residual errors can likely be attributed to the cross talk between the interferogram channels and retarders' misalignment [15].

3.2 Outdoor tests

The outdoor optical performance of the FTISP system was first evaluated by measuring two cars parked 50 m away. Figure 5(a) shows the experimental 2D S_0 spatial images from the 3D datacubes at various wavelengths. Figure 5(b) is RGB composite image that was generated using the FTISP system's $S_0(\sigma)$ data.

The data presented here were acquired at 10:00 a.m. local time on a cloudy day in November of 2013. The gradual decrease in intensity in the top and bottom edges of the FOV is produced by a mismatch of the imaging size of the reimaging lenses (11 mm) with the sensor size of the CCD camera (12.288 mm along the vertical).



Fig. 5. (a) 2D S_0 spatial images from the 3D datacubes at various wavelengths. (b) RGB composite image that was generated using the FTISP system's spectral data.

Figure 6(a) shows the experimental 2D degree of polarization (DOP) spatial images from the 3D datacubes at various wavelengths. Figure 6(b) is band integrated DOP data. The DOP is calculated from S_0 , S_1 , S_2 and S_3 using [4]

DOP(
$$\sigma$$
) = $\frac{\sqrt{S_1(\sigma)^2 + S_2(\sigma)^2 + S_3(\sigma)^2}}{S_0(\sigma)}$. (12)

The black Audi car is brighter than the white car in the DOP band integrated data since the DOP of the black car is higher than the white car's.

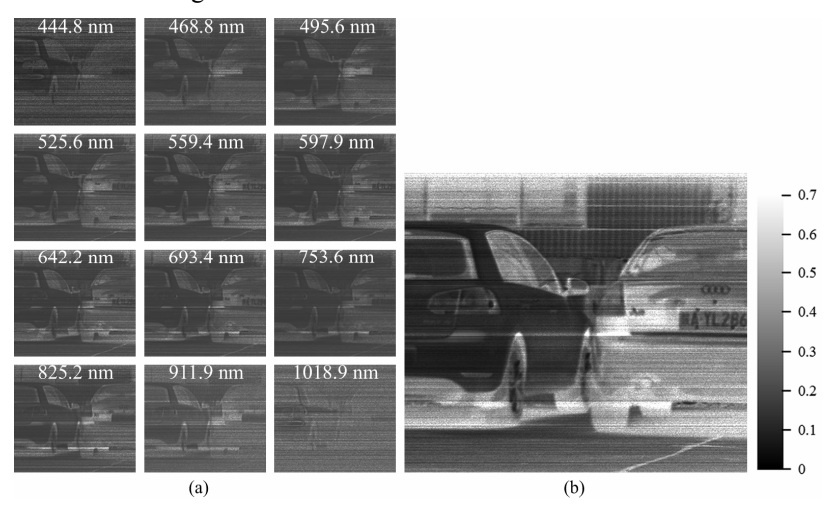


Fig. 6. (a) 2D DOP spatial images from the 3D datacubes at various wavelengths. (b) DOP, band integrated data.

Another test data from the FTISP proof of concept sensor have been collected for three potted flowers, include artificial and natural ones. The obtained RGB composite image and spectra for artificial and natural leaves of the flowers are depicted in Fig. 7. Note that the natural leaves' spectrum increases past 700 nm due to chlorophyll. Figure 8 shows DOP band integrated data and S_0 spatial image at 753.6 nm. In the DOP image, leaves of artificial flower

are brighter than those of natural ones. However, in the 753.6 nm band S_0 image the opposite occurs.

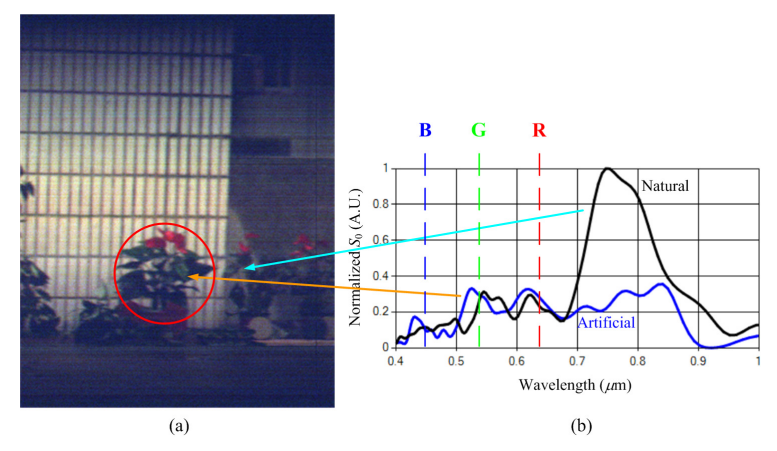


Fig. 7. (a) RGB composite image that was generated using the FTISP system's spectral data (Artificial flower is indicated by red circle). (b) Spectra for artificial and natural leaves.

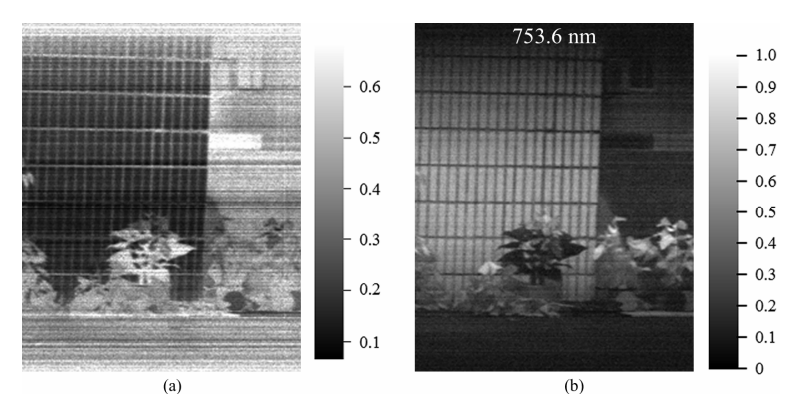


Fig. 8. (a) DOP, band integrated data. (b) S_0 image at 753.6 nm wavelength.

4. Conclusion

We have demonstrated a technique and constructed a Fourier-transform ISP to obtain the full wavelength-dependent state of polarization, spectral and spatial information of a scene with no internal moving parts, electrically controllable or micro-components. The ISP is based on channeled polarimetry and a static Wollaston interferometer. Laboratory test experiments of a uniform light source and a broadband polarizer have demonstrated the spectropolarimetric capability of the instrument. Outdoor test images of cars, artificial and natural plants have proved the system could acquire high quality wavelength-dependent degree of polarization, spectral and spatial data of a scene. Experimental results on artificial and natural plants measurements further demonstrated the practicability of the FTISP system for color measurement, target identification, and agriculture monitoring applications. The FTISP system holds great potential as a practical and versatile tool to meet the needs of spectral and polarization information in industrial and scientific fields.

Acknowledgments

The research was supported by the National Natural Science Foundation of China (Grant No. 61205187) and the China Postdoctoral Science Foundation (Grant No. 2012M510217).